Proceedings of the International Gas Turbine Congress 2003 Tokyo
November 2-7, 2003

IGTC2003Tokyo TS-058

Effects of Airfoil Clocking on Aero-performance and Unsteady Blade Loading in a High-Speed Axial Compressor

Dai KATO[1] and Kuniyuki IMANARI[2]

[1] Advanced Technology Department, Aero-Engine&Space Operations,
Ishikawajima-Harima Heavy Industries Co., Ltd.
229 Tonogaya, Mizuho-machi, Nishitama-gun, Tokyo 190-1297, JAPAN
Phone: +81-42-568-7420, Fax: +81-42-568-7247, E-mail: dai_kato@ihi.co.jp
[2] Ishikawajima-Harima Heavy Industries Co., Ltd.

ABSTRACT

This paper investigates numerically the effects of airfoil clocking on aero-performance and unsteady blade loading in low-speed and high-speed compressor rotor-stator-rotor stages using a quasi-3D unsteady multi-stage Navier-Stokes code. In each of the 1.5-stage cases, four computations are performed at different clocking positions between the upstream rotor and the downstream rotor, in 25% blade-pitch increment. Computation of the low-speed case shows that the maximum efficiency is achieved when the upstream rotor wake impinges on the leading edge of downstream rotor, a similar efficiency variation trend with that of the previous studies for low-speed cascades. The high-speed case, on the other hand, indicates different efficiency variation trend from the low-speed case. Underlying mechanism is related to the change in the downstream rotor blade suction-surface shock strength depending on the path of the upstream rotor blade wake through the downstream rotor blade-to-blade passage. Furthermore, due to the change in the rotor shock strength, unsteady loading on the stator vane in between the two rotors is found to vary significantly. The present computation's ability to predict unsteady vane-surface pressures is also validated using in-house rig test data.

INTRODUCTION

Airfoil clocking has been investigated recently by several researchers, for it possesses an attractive efficiency improvement potential for turbomachinery without any design changes on the airfoils. In turbines, Huber, et al (1995) measured 0.8 point efficiency variation in a two-stage turbine by clocking the first stage stator relative to the second stage stator. Griffin, et al (1995) obtained a maximum efficiency at the same clocking position by conducting a 2-D unsteady Navier-Stokes analysis at the mid span of the same turbine. Arnone, et al (2001) reported, using a quasi-3D unsteady N-S analysis, a 0.7 point efficiency variation by clocking the rotors and the stators of a three-stage low pressure turbine.

For compressors, effects of stator clocking were investigated numerically by Gundy-Burlet, et al(1997) for a low-speed 2.5 stage case using a 2-D N-S analysis. Dorney, et al (1998) studied a mid-subsonic 1.5 stage case using a quasi-3D N-S analysis. These studies reported roughly 0.6 point efficiency variations. In an experimental study by Saren, et al (1998), 0.8 point efficiency variation was reported by clocking the inlet guide vanes and the downstream stator vanes in a high-subsonic 1.5 stage machine.

One of the major conclusions from these studies is that the maximum performance is achieved when the upstream airfoil wake impinges on the leading-edge of downstream airfoil in the same frame of reference. These studies are however mostly limited to low-speed configurations, and question remains whether the same effect can be found in high-speed compressor stages. A recent study by He, et al (2002) using an efficient multi-stage, single-passage harmonic solver revealed a different loss variation trend by rotor-rotor clocking in a transonic flow compared to the trend in a subsonic flow. Even though their explanation that the loss variation in the transonic case was related to interaction between the upstream rotor wake and the downstream rotor suction-surface shock was very interesting, it lacked detailed supporting evidence, partly because of the simplified analysis approach.

One of the concerns for applying clocking in compressors is its effect on the unsteady blade loading on the middle airfoil in between the upstream and downstream airfoils. Cizmas, et al (1999) showed by a quasi-3D unsteady N-S study on IGV-rotor –stator configuration that unsteady pressure on the rotor at the maximum efficiency IGV-stator position could be more than three-times larger in magnitude than at the minimum efficiency position. Hsu, et al (1997) reported in their experimental study that by clocking the rotors in a low-speed rig, the unsteady force on the stator could be changed by more than 60%. Question remains whether such variation in blade forces could be observed in high-speed cases as well.

This paper investigates the effects of airfoil clocking on performance in both high-speed and low-speed compressor rotor-stator-rotor stages using a quasi-3D unsteady multi-stage Navier-Stokes code. In the high-speed case, an efficiency variation mechanism, unique for transonic flow, is described, which is related to the change in the downstream rotor blade suction-surface shock strength depending on the path of the upstream rotor blade wake through the downstream rotor blade-to-blade passage. Furthermore, variation of the unsteady loading on the stator vane in between the two rotor blade rows is studied for the transonic case to see the effects of rotor clocking on its aeromechanics.

COMPRESSOR CASCADES

As shown in Fig.1, two 1.5-stage cases are extracted for the present study from an advanced research multistage high-pressure compressor. All the computations are conducted at the mid-span.

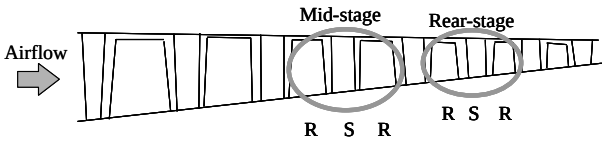

Fig. 1 Cross-section of an advanced research HPC and mid- and rear-stages for clocking study

Manuscript Received on April 15, 2003

Table 1 Specifications for subsonic 1.5-stage case

	Upstream rotor	Middle stator	Downstream rotor
Airfoil count ratio	3	4	3
Solidity	1.64	1.70	1.60
Mach number	0.75	0.56	0.74
Pressure ratio	1.34	-	1.28
AVDR	1.090	1.078	1.077
Reynolds number 10^6	1.79	1.22	2.08

Table 2 Specifications for transonic 1.5-stage case

	Upstream rotor	Middle stator	Downstream rotor
Airfoil count ratio	5	8	5
Solidity	1.70	1.61	1.77
Mach number	0.91	0.80	0.85
Pressure ratio	1.62	-	1.47
AVDR	1.212	1.123	1.163
Reynolds number 10^6	1.53	0.94	2.02

The rear 1.5-stage represents low-speed or subsonic configuration, where as the mid 1.5-stage represents high-speed or high-subsonic to transonic configuration. Table 1 and Table 2 show their main aerodynamic and geometric design parameters. For the high-speed case, flow enters both the upstream and the downstream rotors with subsonic relative Mach number, and become supersonic near their suction surfaces, locally creating shock waves.

NUMERICAL PROCEDURE

The numerical scheme and the grid system used in this study were originally developed and validated by Outa, et al (1994) using a subsonic compressor rig test data. The scheme was applied afterwards to transonic rotor-stator system and its ability to predict rotor wake profile and the downstream stator vane surface pressure was validated. Comparison of the computed stator vane unsteady pressure with the in-house rig test data is made in later section. Summary of the numerical system is described below.

Governing flow-field equations at mid span are approximated by quasi-3D unsteady Reynolds-averaged Navier-Stokes equations, assuming that the flow is parallel to a stream-tube. A two-layer algebraic turbulence model by Baldwin and Lomax (1978) is used for turbulence closure. A third-order upstream TVD finite difference scheme of Chakravarthy-Osher (1985) is applied for the convective terms. A second-order central finite-difference is applied for viscous terms. A first-order Euler backward scheme is used for temporal discretization with a relatively small global time step width, and Newton-Raphson sub-iteration is applied to reduce the linearization and factorization errors in the time integration.

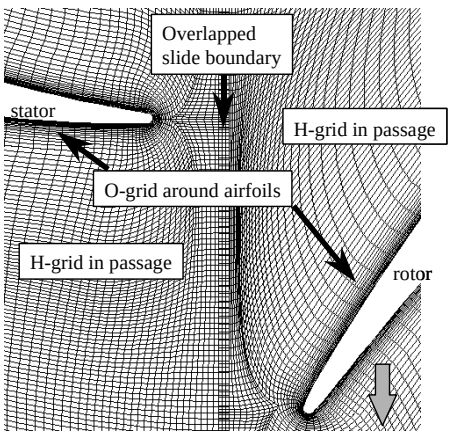

Fig.2 Numerical grid system for unsteady stage analysis

As shown in Fig.2, a structured computational grid system is constructed with an O-grid around the airfoils and an H-grid filling the rest of the passages. Normal grid width on the surface is kept to y+=3-5. Number of grid points for each of the O-grid is 201x21, while for the H-grids in the transonic case, 151x51(axial x circumferential) nodes are provided per passage for the upstream rotor, 131x121 per passage for the stator, and 141x151 per passage for the downstream rotor. The middle stator and the downstream rotor domains are densely discretized to capture the upstream rotor wakes. Total number of grid points is around 350,000 for 5-rotor-blade/8-stator-vane/5-rotor-blade case. Note that the B-L turbulence model is solved not only in O-grids but also in H-grids by handing over information at the grid interfaces. The model is, however, applied only around the airfoils, and not in the wakes.

On the inlet boundary, total pressure, total temperature and absolute flow angle are specified, and static pressure is specified on the exit boundary. At the overlapped sliding boundary between the rotor and the stator domains, boundary conditions at one domain are obtained by simply linear-interpolating locally the physical variables from the other domain at each time step. Cyclic boundary condition is applied on the circumferential periodic boundary. No-slip and adiabatic condition are assumed on the airfoil surfaces.

As shown in Fig.3, the downstream rotor blade is clocked with respect to the upstream rotor blade. Four clocking positions, designated as shift=0%pitch, 25%pitch, 50%pitch, and 75%pitch, are computed for each of the cases.

PREDICTED PERFORMANCE VARIATION FOR SUBSONIC CASCADE CASE

Figure 4 shows the variation in efficiency with respect to the clocking position for the rear-stage subsonic case. Here, efficiency h is calculated using Eq.(1):

$$h = \frac{\left(\overline{\overline{\frac{P_{t,ex}}{P_{t,in}}}}\right)^{(g-1)/g} - 1}{\overline{\overline{\frac{T_{t,ex}}{T_{t,in}}}} - 1} \qquad (1)$$

where P_t, T_t and g indicate absolute total pressure, absolute total temperature and specific heat ratio, respectively. Subscripts *in* and *ex* respectively indicate inlet and exit, while $\overline{(\ )}$ and $\overline{\overline{(\ )}}$ indicate spatial-average and time-average. Spatial averaging at the stage inlet is mass-weighted, while at the stage exit, mixed-out averaging is performed to take mixing loss into account; see Appendix for detail of the averaging processs. It is found that the maximum efficiency as a whole, as well as for the downstream rotor blade alone, is achieved at shift=25% position. Figure 5(a) shows the phase-lock averaged entropy field at this clocking position. The upstream rotor blade wake is seen to impinge on the leading-edge

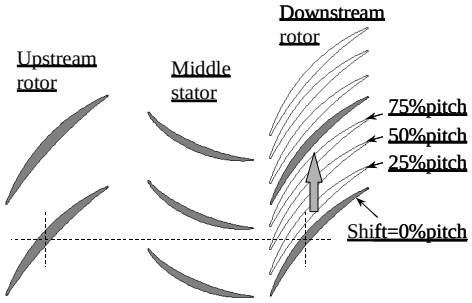

Fig.3 Definition of clocking positions

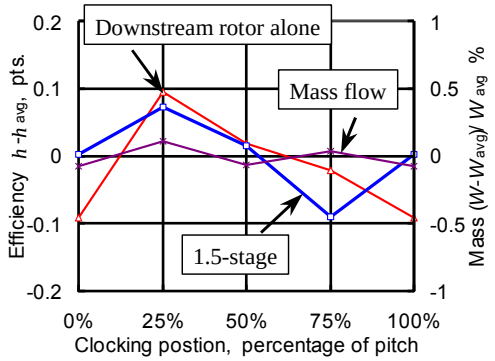

Fig.4 Variation of predicted efficiency against clocking position for rear-stage subsonic case.

of the downstream rotor blade. Such an observation is in accordance with findings from other published papers. Only 0.2point efficiency variation is predicted for this case. One reason for the small difference in efficiency among the clocking positions may be attributed to the wake trajectory of the upstream rotor blades being disturbed by the vortices shed from their trailing edges under this computed condition; see Fig.5 (b). Reynolds number based on the relative flow velocity at the rotor exit and the rotor blade trailing edge radius is around 1.0×10^4, which indicates that such a Karman-like vortex shedding may be possible if the trailing

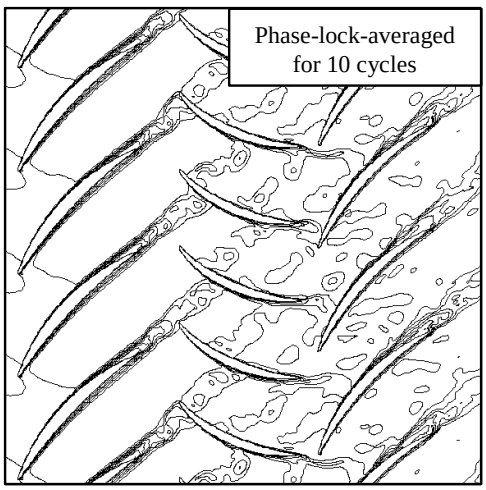

(a) Phase-lock averaged entropy field

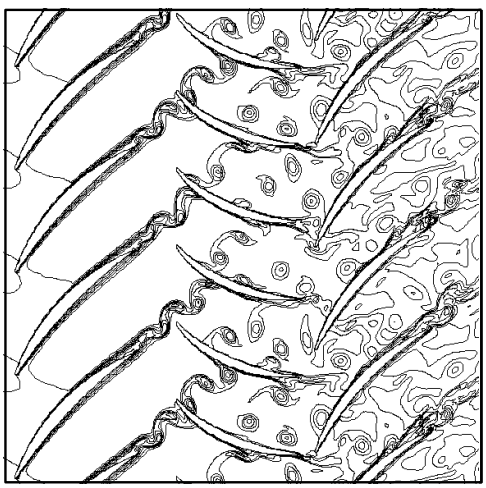

(b) Instantaneous entropy field

Fig.5 Computed flow field at maximum efficiency clocking position (shift=25%pitch) for subsonic case.

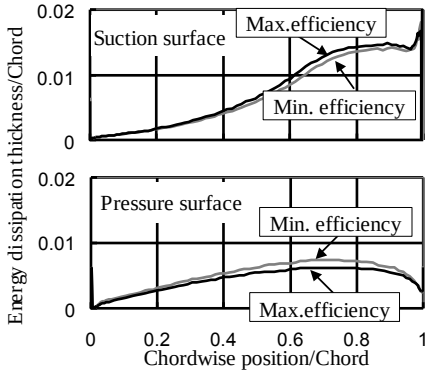

Fig.6 Time-averaged energy dissipation thickness of downstream rotor blade surface boundary layer at max/min positions for subsonic case

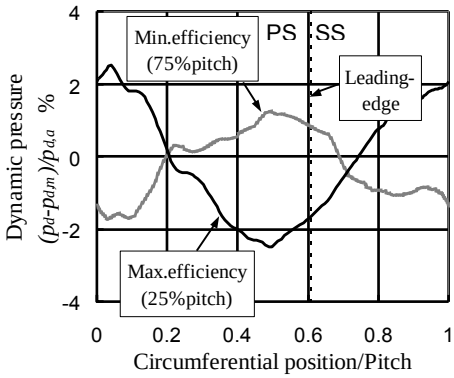

Fig.7 Time-averaged relative dynamic pressure at downstream rotor inlet for subsonic case

edge is thought of as a 2-D circular cylinder. Strouhal number is found to be around 0.16 for the present case. Dense O-grid around the edge region might have enabled the present simulation to capture such behavior. This type of vortex shedding is not, however, observed for the transonic case in the next section, although the Reynolds number is about the same with that of the present case. Further study is needed to clarify the reason for such wake behavior. Lack of wake model in the present Baldwin-Lomax simulation is another candidate that caused this type of wake behavior.

Figure 6 shows the energy dissipation thickness d_3 of the boundary layer on the downstream rotor blade surfaces. Here, d_3 is calculated by Eq.(2) using the time-averaged quantities:

$$d_3(s)=\int_0^d \frac{\bar{\bar{r}}(s,n)\bar{\bar{u}}(s,n)}{\bar{\bar{r}}_e(s)\bar{\bar{u}}_e(s)}\left(1-\frac{\bar{\bar{u}}^2(s,n)}{\bar{\bar{u}}_e^2(s)}\right)dn \qquad (2)$$

where r, u, and d indicate density, relative flow velocity, and boundary layer thickness, respectively, while s and n respectively indicate surface-wise distance from the leading edge and a local coordinate normal to the blade surface. Subscript e denotes quantities at the edge of the boundary layer. As shown in the figure, no significant difference in energy dissipation thickness of the downstream rotor blade surface is found between the maximum efficiency (25%pitch) and minimum efficiency (75%pitch) cases, indicating no significant difference in loss coefficient between them. On the other hand, the time-averaged dynamic pressure at the leading edge position of the downstream rotor, Fig.7, becomes nearly minimum at the maximum efficiency case and nearly maximum at the minimum efficiency case. Since total pressure loss is the product of loss coefficient and dynamic pressure, the efficiency drop is thought to be related with the difference of

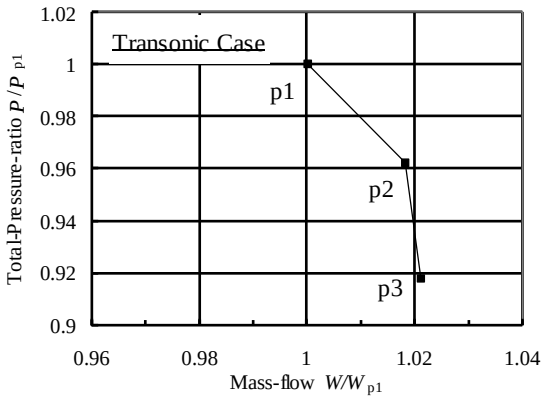

Fig.8 Computed operating points for transonic 1.5-stage case

dynamic pressure at the rotor leading edge.

PREDICTED PERFORMANCE VARIATION FOR TRANSONIC CASCADE CASE

For the transonic case, three operating points, **p1**, **p2** and **p3** are computed as indicated in Fig.8.Efficiency variation mechanism is discussed in detail using the results at **p1**, followed by brief discussion on the effect of loading on optimum efficiency position.

Figure 9 shows the predicted efficiency variation with respect to the clocking position for the mid-stage transonic case **p1**. For this case, maximum efficiency is reached at shift=0%pitch clocking position and minimum efficiency is reached at shift=50%pitch clocking position. Variation in efficiency is computed to be 0.4points for 1.5-stage. Downstream rotor alone shows 1.4-point efficiency change. A slight difference in the computed mass flow among the four clocking positions should have caused some variation for upstream rotor efficiency (negative incidence for higher mass flow cases, shift =0% and 75%pitch clocking positions caused some loss increase). This variation would diminish if the mass flow were adjusted, possibly bringing the 1.5-stage efficiency variation level closer to the downstream rotor alone efficiency variation level.

Figure 10 shows the computed flow fields for the maximum and minimum efficiency clocking positions by instantaneous entropy presentation. It is found that the maximum efficiency (shift = 0%pitch) in this transonic case is achieved when the upstream rotor blade wake passes through the downstream rotor blade-to-blade passage near the suction surface. On the other hand, minimum efficiency (shift = 50%pitch) is achieved when the upstream rotor blade wake passes through the downstream rotor blade-to-blade passage closer to the pressure surface. As shown in

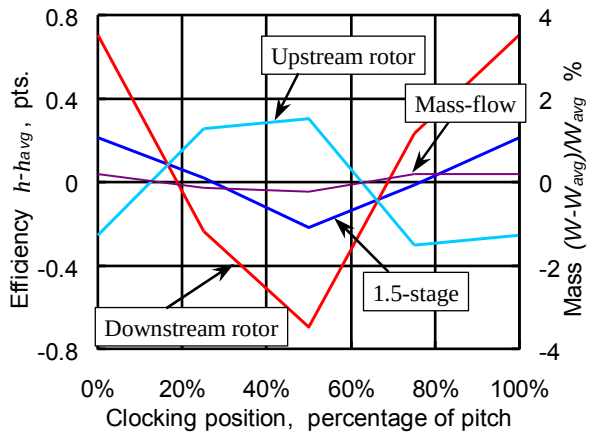

Fig.9 Variation of predicted efficiency against clocking position for transonic mid-stage case, operating point **p1**

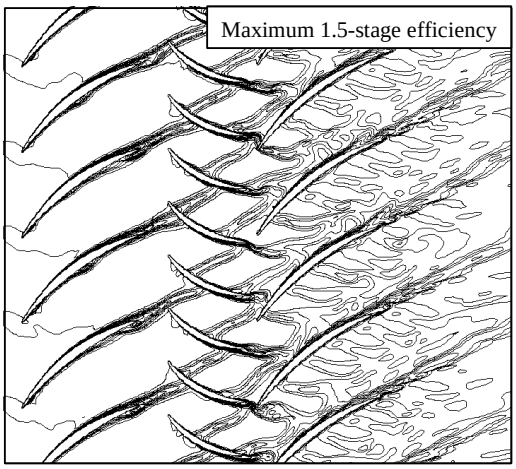

(a) Shift = 0%pitch (maximum efficiency)

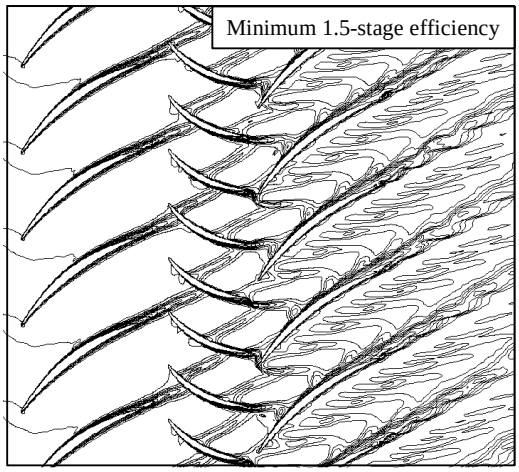

(b) Shift = 50%pitch (minimum efficiency)

Fig.10 Computed instantaneous flow field for mid-stage transonic case **p1** (entropy contours)

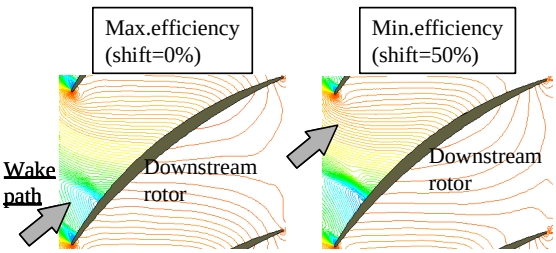

(a) Time-averaged pressure contours

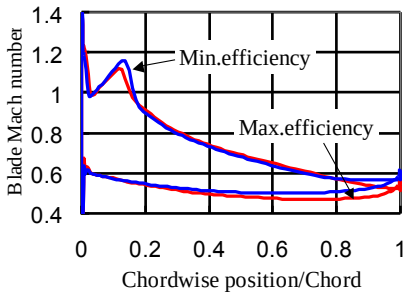

(b) Time-averaged isentropic Mach number

Fig.11 Difference in strength of suction-surface shock of downstream rotor blade at maximum and minimum clocking positions; mid-stage transonic case.

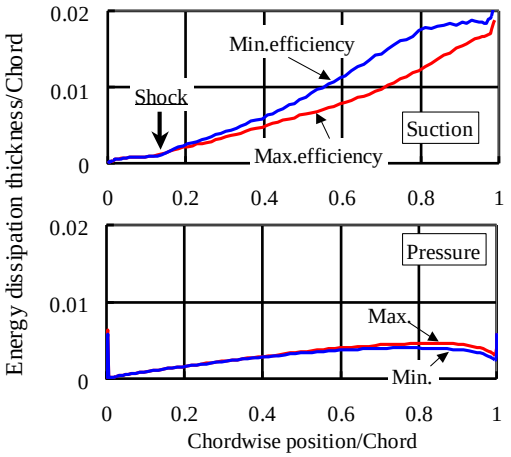

(a) Energy dissipation thickness of downstream rotor

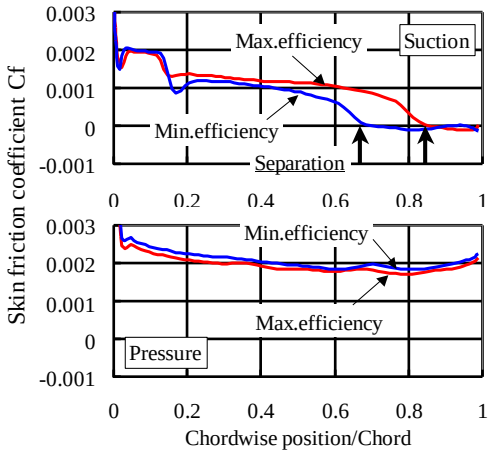

(b) Skin friction coefficient of downstream rotor

Fig.12 Time-averaged boundary-layer characteristics of downstream rotor blade at maximum and minimum clocking positions in mid-stage transonic case

Fig.11(a) by the time-averaged pressure contours and in Fig.11(b) by the time-averaged blade surface Mach number distribution, the shock wave on the suction surface of the downstream rotor blade is weaker in the maximum efficiency clocking position than in the minimum efficiency position. Such a difference in the shock strength is found to be caused by the difference in the relative inlet Mach number near the suction surface of the downstream rotor blade. In the maximum efficiency case, lower Mach number flow of the upstream rotor blade wake passes over the suction surface, compared to the minimum efficiency case when the wake passes near the pressure side.

Due to the weakened shock wave, the energy dissipation thickness on the suction surface of the downstream rotor blade is found not to grow as drastically behind the shock foot as in the minimum efficiency case, as shown in Fig.12(a), thus contributing to the suppression of the loss increase of the downstream rotor blade. In addition, weakened shock is found also to delay the suction surface flow separation toward the trailing-edge for the maximum efficiency case; see Fig.12(b).

He, et al (2002) observed in their transonic rotor-stator-rotor CFD that the maximum loss, or the minimum efficiency, was obtained when the upstream rotor wake passed over the suction surface of the downstream rotor, which was contrary to the present result. They stated that at this clocking position, the upstream rotor wake passed across the strongest part, i.e. the foot, of the downstream rotor passage shock among other positions, resulting in most severe deceleration of the wake fluid and highest mixing loss. Their nonlinear harmonic CFD, on the other hand, seems not

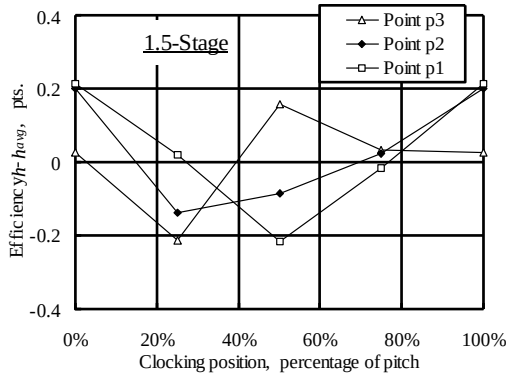

(a) 1.5-stage efficiency variation

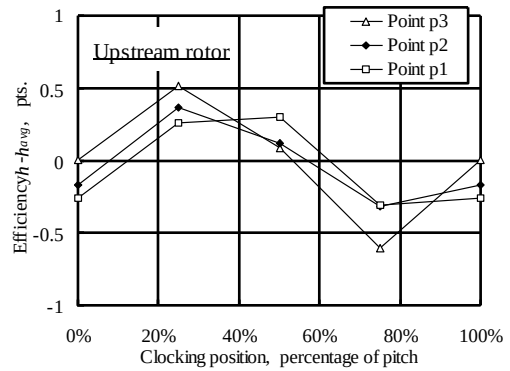

(b) Upstream rotor efficiency variation

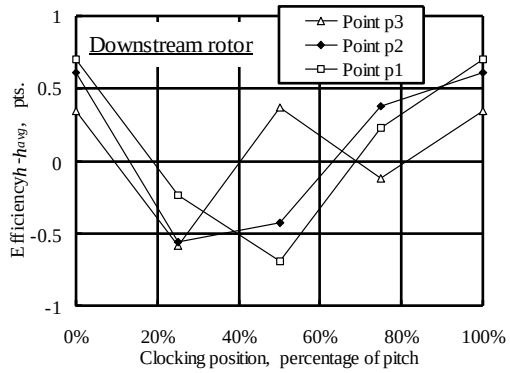

(c) Downstream rotor efficiency variation

Fig.13 Effect of loading on computed efficiency variation with respect to clocking position for transonic case.

to have predicted the weakening of the shock foot due to coming of the lower inlet Mach number flow of the upstream rotor wake, as mentioned in the present case. It may be assumed that, at this clocking position, the present case predicted the decrease of the downstream rotor blade profile loss due to the shock weakening to be larger than the increase of the upstream rotor wake mixing loss described by He, et al. Such difference in the optimum clocking position between the two computations is believed to be largely due to the difference in the Mach number. The computation by He, et al, is done for the front stage of a transonic compressor, so that the incoming Mach number should be higher and the shock stronger and more developed than in the present case. Difference in the Mach number level may determine which loss mechanism overrides the other in the downstream rotor region. Adequacy of the present computation to accurately predict He's loss mechanism should also be addressed in the authors' future research.

Figure 13 summarizes the effect of loading on the efficiency variation trend with respect to rotor clocking for the transonic case.

Maximum efficiency is achieved at roughly the same clocking position (shift=0%pitch) at **p2** and **p1**, indicating that clocking is not sensitive to loading for moderate to high loading conditions in the computed case. Optimum clocking position for low loading condition **p3** is changed to shift=50%. Computed data showed some overturning of the upstream rotor exit flow at **p3** compared to **p1** and **p2** cases, which resulted in change of the upstream rotor wake circumferential position at the downstream rotor blade inlet. Such overturning at **p3** resulted from the upstream rotor inlet flow being more negative incidence than in **p1** and **p2**, causing more attached flow on the suction surface, while producing some flow separation on the pressure surface.

UNSTEADY BLADE LOADING

Clocking is reported to accompany variation in the amplitude of the unsteady loading on the middle blade/vane in between the upstream and downstream vane/blade rows. In this section, unsteady aerodynamic loading on the middle stator vane in the present transonic 1.5 stage case is studied using the computed data.

Before analyzing the vane surface pressure data in the present transonic case, the present numerical code is validated first for its ability to predict such unsteady pressures. Another computation is performed at the mid-span of a single-stage transonic axial compressor, in which a series of rig test has been performed in-house to obtain unsteady pressure data on the stator vane surface generated by the upstream rotor blade wakes. Unsteady pressure was measured by flush mounting arrays of pressure transducers at the mid span of the stator vane's suction and pressure surfaces. Details are described in Kato, et al (1999). Figure 14 shows the computed flow field using the present numerical code. Computed

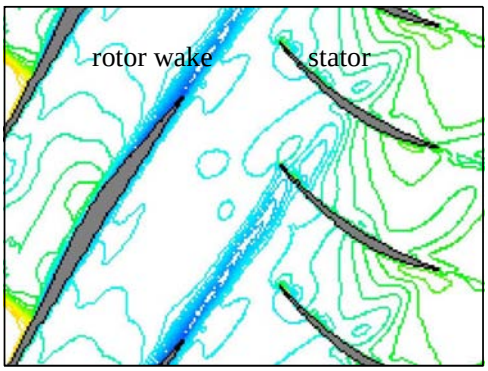

Fig.14 Computed flow field of an in-house single-stage axial compressor; relative Mach number contour (mid-span, 75%design speed , design load)

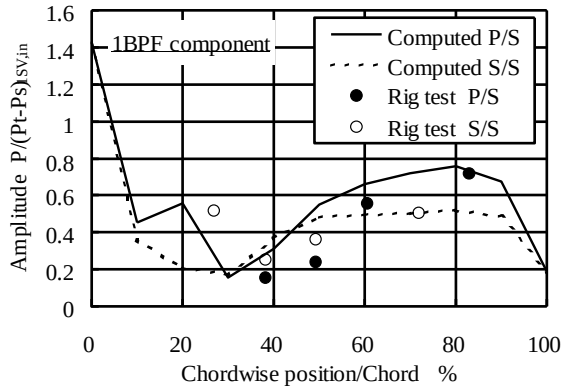

Fig.15 Comparison of computed stator vane unsteady pressure amplitude to measured data from of single-stage compressor rig test(Kato, et al 1999); 75%design speed, design-load, mid-span.

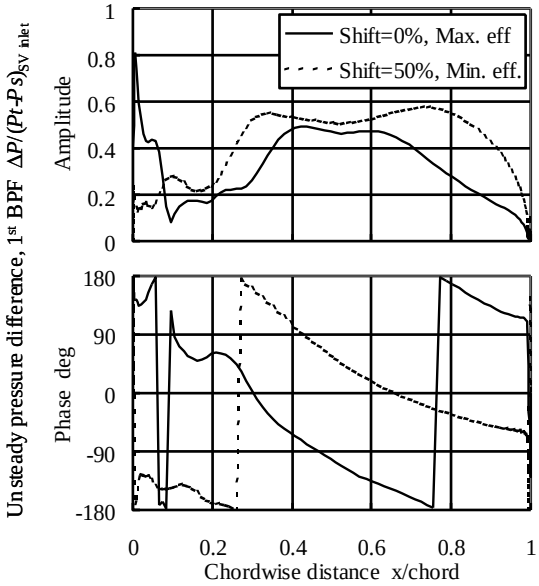

Fig.16 Comparison of computed unsteady loading on stator vane of transonic 1.5 stage case, operating point **p2**, between different rotor clocking positions.

time-dependent pressure data on the stator vane is Fourier decomposed to obtain the first blade-passing-frequency (BPF) component, which is usually of primary concern from an aeromechanical viewpoint. Figure 15 compares the chord-wise distribution of the predicted and measured pressure amplitudes of the 1st BPF component for 75%design speed case. It can be seen that the present numerical code predicts the vane surface unsteady pressure fairly well.

Returning to the transonic 1.5-stage case, Fig.16 compares the chord-wise distribution of the unsteady pressure difference on the stator between different clocking positions. These are the averaged profile over the eight vanes in the stator. Here, the unsteady pressure difference is defined as the difference of the pressure between the pressure surface and the suction surface at the same percentage of the surface-wise distance from the leading edge. Specifically, it is calculated as follows;

$$
\begin{aligned}
dP_{s,R}(s) &= \tilde{P}_{s,ps}(s)\cos f_{ps}(s) - \tilde{P}_{s,ss}(s)\cos f_{ss}(s) \\
dP_{s,I}(s) &= \tilde{P}_{s,ps}(s)\sin f_{ps}(s) - \tilde{P}_{s,ss}(s)\sin f_{ss}(s) \\
Amplitude &= \sqrt{dP_{s,R}{}^2 + dP_{s,I}{}^2} \\
Phase &= \tan^{-1}\left(dP_{s,R} \Big/ dP_{s,I} \right)
\end{aligned}
\qquad (3)
$$

where $\tilde{P}_s$ and f denote amplitude and phase of the first BPF Fourier coefficient of the static pressure on the stator vane, s denotes surface-wise distance from the leading edge, and subscripts ps and ss denote pressure surface and the suction surface.

It is found from Fig.16 that, in this transonic case, unsteady loading is much larger at the minimum efficiency clocking position, shift =50%pitch, than at the maximum efficiency clocking position, shift =0%pitch. This is somewhat contrary to previous observations for low speed cases in open literature, for example Cizmas, et al (1999), that higher unsteady loading is usually generated at maximum efficiency position. An explanation for the variation in unsteady loading for the present case is related to the difference in the shock strength on the suction surface of the downstream rotor blade as mentioned in the last section. As shown in Fig.17, stronger shock waves are seen for shift=50%pitch clocking position than for shift=0%pitch clocking position, which is again due to the

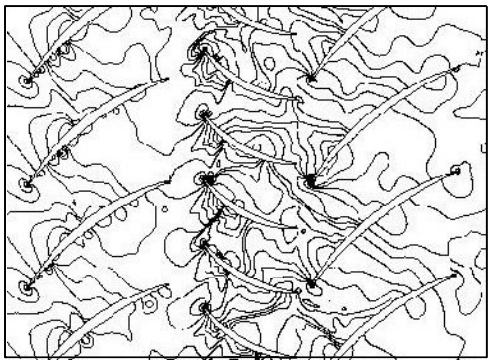

(a) Shift = 0%pitch

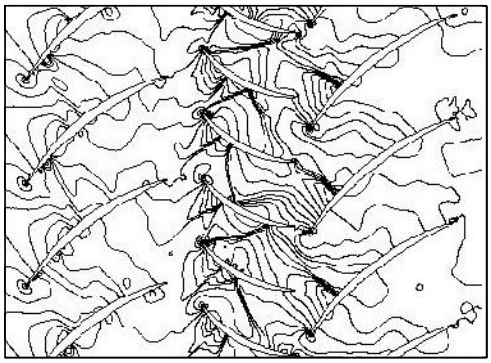

(b) Shift = 50%pitch

Fig.17 Comparison of computed pressure field for two clocking position; transonic 1.5-stage case, **p2**.

difference in the circumferential position of the upstream rotor blade wake at the downstream rotor inlet. Due to the stronger shock wave, stronger potential disturbance response is generated on the upstream stator for shift=50%pitch case.

Such an unsteady load variation mechanism attributed to the variation of the downstream rotor blade shock strength by interaction with the upstream rotor blade wake flow is thought to be unique to high-speed rotor/stator/rotor cascade system as studied in the present paper, and has not been mentioned in previous papers on low speed cascades, for example Hsu, et al (1997). Present numerical results indicate that it may be possible by clocking to achieve higher efficiency and lower unsteady loading at the same time in transonic rotor-stator-rotor configuration.

CONCLUSIONS

Effects of airfoil clocking on aerodynamic performance and unsteady loading in subsonic and transonic 1.5-stage rotor-stator-rotor cases in multistage axial compressor are investigated using a quasi-3D unsteady Navier-Stokes simulation. Following findings are obtained from the present study:

(1) In the rear-stage subsonic case, maximum efficiency is obtained when the upstream rotor blade wakes impinge on the leading edges of the downstream rotor blades. This is in accordance with previous findings in open literature. Efficiency variation in the computed case is only 0.2points.

(2) In the mid-stage transonic case, maximum efficiency is attained when the upstream rotor blade wake passes through the downstream rotor blade-to-blade passage near the suction surface. At this clocking position, strength of the suction surface shock of the downstream blade is weakened due to the lower Mach number flow of the upstream rotor blade wake passing over the suction surface. Profile loss behind the shock foot stays at a lower level than in the minimum efficiency, shift = 50%pitch, case, in which the shock is intensified by higher Mach number main flow over the suction surface. Computed 1.5-stage efficiency variation is 0.4points.

(3) Clocking is found to be relatively insensitive to loading for the computed transonic case for moderate to high loading condition.

(4) The present numerical code is validated using in-house rig test data for prediction of unsteady blade loading. Unsteady pressure on the middle stator vane of the transonic 1.5-stage case is then investigated. Due to the weaker shock of the downstream rotor blade, as mentioned in (2), weaker potential response is observed for the maximum efficiency, shift=0%pitch clocking position, than in the minimum efficiency, shift=50%pitch clocking position. It may be possible in transonic configurations to attain high efficiency and low unsteady blade loading at the same clocking position.

ACKNOWLEDGEMENT

The authors would like to acknowledge Mr. Kazumasa Tsuboi of IHI-Scube for conducting the numerical analyses and post-processing.

REFERENCES

Arnone, A., Marconcini, M., Pacciani, R., Schipani, C., Spano, E., 2001, "Numerical Investigation of Airfoil Clocking in a Three-Stage Low Pressure Turbine," ASME Paper 2001-GT-0303.

Baldwin, B. S. and Lomax, H., 1978, "Thin Layer Approximation and Algebraic Model for Separated Turbulent Flows," AIAA-78-257.

Chakravarthy, S. R. and Osher, S., 1985, "A New Class of High Accuracy TVD Schemes for Hyperbolic Conservation Laws," AIAA-85-0363.

Cizmas, P. G. and Dorney, D. J., 1999, "The Influence of Clocking on Unsteady Forces of Compressor and Turbine Blades," 14th International Symposium on Air Breathing Engines, ISABE-99-7231.

Dorney, D. J., Sharma, O. P., and Gundy-Burlet, K. L., 1998, "Physics of Airfoil Clocking in a High-Speed Axial Compressor," ASME Paper 98-GT-82

Griffin, L. W., Huber, F. W., and Sharma, O. P., 1995, "Performance Improvement through Indexing of Turbine Airfoils Part2 – Numerical Simulation," ASME Paper 95-GT-28.

Gundy-Burlet, K. L. and Dorney, D. J., 1997, "Physics of Airfoil Clocking in Axial Compressors," ASME Paper 97-GT-444.

He, L., Chen, T., Wells, R. G., Li, Y. S., and Ning, W., 2002, "Analysis of Rotor-Rotor and Stator-Stator Interferences in Multi-Stage Turbomachines," ASME Paper GT-2002-30355.

Hsu, S. T. and Wo, A. M., 1997, "Reduction of Unsteady Blade Loading by Beneficial Use of Vortical and Potential Disturbances in an Axial Compressor with Rotor Clocking," ASME Paper 97-GT-86.

Huber, F.W., Johnson, P. D., Sharma, O. P., and Gaddis, S. W., 1995, "Performance Improvement through Indexing of Turbine Airfoils Part1 – Experimental Investigation," ASME Paper 95-GT-27.

Kato, D., Watase, T., Hattori, H., Kobayashi, K., and Mizuta, I., 1999, "Prediction of High-Order-Mode Blade Forced Response in a Transonic Axial Compressor," 14th International Symposium on Air Breathing Engines, ISABE-99-7031.

Outa, E., Kato, D., and Chiba, K., 1994, "An N-S Simulation of Stall Cell Behavior in a 2-D Compressor Rotor-Stator System at Various Loads," ASME Paper 94-GT-257.

Saren, V. E., Savin, N. M., Dorney, D. J., and Sondak, D. L., 1998, "Experimental and Numerical Investigation of Airfoil Clocking and Inter-Blade-Row Gap Effects on Axial Compressor Performance," AIAA-98-3413.

APPENDIX

In order to evaluate 1.5-stage efficiency using Eq.(1), following averaging procedure is performed. Flow quantities are spatial averaged first at each time step. At the stage inlet, this spatial averaging is mass-weighted, as expressed in Eq.(A1), since

no mixing processs takes place in front of the upstream rotor.

$$\bar{f} = \int_0^{S_{in}} r v_m f dy / S_{in} \qquad \text{(A1)}$$

Here, f is the flow quantity to be averaged, v_m is the meridional velocity, y is the circumferential coordinate, and S_{in} is the circumferential length of the computed domain at the inlet.

At the stage exit, mixed-out averaging is performed to take mixing loss into account. The mixed-out averaged density, meridional flow velocity, circumferential flow velocity v_q , and static pressure P_s are obtained by solving the following set of equations (A2);

$$\begin{aligned}
&\overline{\overline{r}\,\overline{v_m}} S_{ex} = \int_0^{S_{ex}} r v_m dy \\
&\left(\overline{\overline{r}\,\overline{v_m}^{\,2}} + \overline{P_s} \right) S_{ex} = \int_0^{S_{ex}} \left(r v_m^{\,2} + P_s \right) dy \\
&\overline{\overline{r}\,\overline{v_m}\,\overline{v_q}} S_{ex} = \int_0^{S_{ex}} r v_m v_q \, dy \qquad \text{(A2)} \\
&\left[\frac{g\,\overline{P_s}}{g-1} + \frac{1}{2}\left(\overline{\overline{v_m}^{\,2}} + \overline{\overline{v_q}^{\,2}} \right) \right] \overline{\overline{v_m}} S_{ex} = \\
&\qquad \int_0^{S_{ex}} \left[\frac{g P_s}{g-1} + \frac{1}{2}\left(v_m^{\,2} + v_q^{\,2} \right) \right] v_m dy
\end{aligned}$$

From the above mixed-out quantities, total pressure and total temperature are calculated.

Time-averaged quantities are obtained by averaging the above spatial-averaged instantaneous quantities over certain time span. In the present study, time span for the rotor blade to travel 25 rotor blade pitches (five sweeps) are taken for the high-speed case, and 30 rotor blade pitches (ten sweeps) are taken for the low-speed case. Data sampling is performed at each time the rotor traveled one-fiftieth of the rotor blade pitches.